Phys Chem Minerals (2003) 30: 256–266
DOI 10.1007/s00269-003-0312-8

ORIGINAL PAPER

E. Thurel · P. Cordier

Plastic deformation of wadsleyite: I. High-pressure deformation in compression

Received: 15 July 2002 / Accepted: 14 February 2003

Abstract We have studied the plastic deformation of Mg_2SiO_4 wadsleyite polycrystals. Wadsleyite was synthesized from a forsterite powder in a multianvil apparatus. It was then recovered and placed in a second multianvil assembly designed to induce plastic deformation by compression between two hard alumina pistons. After the deformation experiment, the microstructures are characterized by transmission electron microscopy (TEM) and large-angle convergent beam electron diffraction (LACBED). Deformation experiments have been carried out at 15–19 GPa and at temperatures ranging from room temperature to 1800–2000 °C. Five different dislocation types have been identified by LACBED: [100], 1/2⟨111⟩, [010], ⟨101⟩ and [001]. The [001] dislocations result from dislocation reactions and not from activation of a slip system. The [010] dislocations are activated under high stresses at the beginning of the experiments and further relax by decomposition into 1/2⟨111⟩ dislocations or by dissociation into four 1/4[010] partial dislocations. The following slip systems have been identified: 1/2⟨111⟩{101}, [100](010), [100](001), [100]{011}, [100]{021}, [010](001), [010]{101} and ⟨101⟩(010).

Keywords Plastic deformation · Dislocation · Slip system · High pressure · TEM

E. Thurel · P. Cordier (✉)
Laboratoire de Structure et Propriétés
de l'Etat Solide, UMR CNRS 8008
Université des Sciences et Technologies de Lille,
Bat C6, 59655 Villeneuve d'Ascq Cedex - France
e-mail: patrick.cordier@univ-lille1.fr
Tel.: +(33)320-43-43 41
Fax: +(33)320-43-65 91

P. Cordier
Bayerisches Geoinstitut,
Universität Bayreuth, Germany

Introduction

Solid-state mantle convection plays a crucial role in the dynamics of the Earth. This phenomenon is controlled to a large extent by the plastic flow behaviour of deep-mantle materials. Together with majorite garnets, the high-pressure polymorphs of olivine, wadsleyite and ringwoodite are believed to be the main constituents of the Earth's transition zone. Despite their importance, little is known about the rheological properties of these minerals in the relevant P, T conditions.

Significant advances have recently been made to investigate the mechanical properties of minerals at high pressures (up to 16 GPa) using the multianvil apparatus (Fujimura et al. 1981; Green et al. 1990; Liebermann and Wang, 1992; Bussod et al. 1993; Dupas et al. 1994; Sharp et al. 1994; Weidner et al. 1994; Cordier et al. 1996; Ando et al. 1997; Karato and Rubie 1997; Chen et al. 1998; Dupas-Bruzek et al. 1998; Durham and Rubie 1998; Karato et al. 1998; Voegelé et al. 1998). The common point of all these experiments is that the sample assembly has been modified in such a way that high differential stresses are generated during compression. Among these studies, some have been devoted to wadsleyite, which is the subject of the present paper. Dupas et al. (1994) transformed a synthetic harzburgite in the β-stability field (14 GPa, 1100–1200 °C). Apart from the stacking faults in (010), relatively few defects are observed in wadsleyite, in contrast with remnant olivine grains, which show high densities of c screw dislocations. The only dislocations observed are emitted at grain boundaries to relax local stress concentrations. The following slip systems have been characterized: [100]{021} (with a predominance of screw segments) and 1/2⟨111⟩{101}. In a further study, Dupas-Bruzek et al. (1998) transformed San Carlos olivine at 900 °C in the β-stability field (15 GPa) for 0.5 h and in the $\beta+\gamma$ stability field (16 GPa) for 11 h. As in the previous

study, dislocations are mostly found in remnant olivine grains. In wadsleyite, dislocations with [100] and $1/2\langle 111\rangle$ Burgers vectors are observed. [100] dislocations are arranged in subgrain boundaries, which led the authors to suggest that recovery by dislocation climb is active in wadsleyite at 900 °C. Higher dislocation densities were introduced in wadsleyite by Sharp et al. (1994), who transformed San Carlos olivine at pressures of 14 GPa and greater and 1450 °C. Long annealing time at pressure and temperature were chosen to allow for significant creep to take place. Dislocations commonly occur in walls although tangles are also observed. The Burgers vectors are found to be [100], and orientations of dislocation segments in subgrain boundaries suggest (010) as a slip plane. The strength of wadsleyite of forsterite composition has been probed in situ in a DIA-type cubic-anvil apparatus by monitoring X-ray diffraction peak broadening as a function of pressure, temperature and time (Chen et al. 1998). Both dry and hydrous (3.8 wt%) samples have been studied. The powder samples are first compressed to 10 GPa at room temperature, then the sample is heated stepwise. The hydrous phase remains as strong as the dry phase at temperatures up to 400 °C where stress relaxation begins. Upon further heating to 600 °C, the hydrous phase begins to weaken relative to the dry phase. Stress drops of 20 and 44% are observed in the dry and hydrous phases, respectively. Indirect information on the strength of wadsleyite was gained by Mosenfelder et al. (2000) by modelling the relaxation of transformation stresses around transforming olivine spheres. The deduced values for the yield strength are between 4 and 6 GPa at 1100 °C and 16–17 GPa. Experiments with nominally dry and water-added samples support the hypothesis that hydrolytic weakening occurs in wadsleyite.

In the present study, we have deformed Mg_2SiO_4 wadsleyite in a multianvil apparatus. Following the procedure described in Cordier and Rubie (2001), the samples are synthesized in a first experiment, and recovered and compressed in a second. The deformation microstructures are characterized by transmission electron microscopy (TEM) and large-angle convergent beam electron diffraction (LACBED). In Part II of this work, similar experiments are described in which the wadsleyite samples are deformed in shear. Finally, the choice of the slip systems and their ease of slip are discussed in Part III on the basis of crystal chemistry and linear anisotropic elasticity considerations.

Experimental details

Synthesis of the wadsleyite samples

The high-pressure experiments were performed at the Bayerisches Geoinstitut with a 6–8 multianvil apparatus (Kawai and Endo, 1970). We used pressure assemblies based on a Cr-doped MgO octahedron containing a cylindrical $LaCrO_3$ resistance heater. The temperature was measured with W3%Re–W25%Re thermocouples inserted axially and placed in contact with the specimen capsule. In the case of thermocouple failure, the temperature (T) was estimated from the power (W) supplied to the heater by using calibration curves $T = f(\mathrm{W})$ previously established for this pressure assembly. We used 10-mm edge length octahedra and 5-mm truncated edge length (TEL) WC cubes for experiments in the pressure range 15–19 GPa. The pressure is determined for this assembly after calibrations previously performed at 1600 °C using the α–β Mg_2SiO_4, the β–γ Mg_2SiO_4 and the coesite-stishovite transitions. The starting material for each synthesis was a forsterite powder fabricated from high-purity oxides, kindly provided by J.L. Mosenfelder. The forsterite powder is placed in a folded Re capsule; long annealing times allowed enhanced grain growth. Indeed, optical examination of the thin sections shows that grains which are several tens or hundreds of micrometres wide are commonly grown. The experimental conditions of the synthesis runs are given in Table 1.

Deformation experiments in the multianvil apparatus

After synthesis, the specimen is recovered and placed in a second high-pressure assembly which is modified in such a way that high differential stresses develop during compression, thus causing the sample to deform. The procedure is described in detail in Cordier and Rubie (2001). Two hard alumina pistons are located at each end of the sample to make the assembly mechanically anisotropic (Fig. 1). The lower piston consists of solid alumina whereas the upper piston acts as the thermocouple sleeve and contains the thermocouple wires. In one case (H1260, see Table 2), the alumina pistons were replaced by solid sapphire pistons. In this case, the temperature was deduced from the $T = f(\mathrm{W})$ calibration curve. Thin (25 μm) Re discs are inserted between the pistons and the polished faces of the sample to avoid chemical reaction between the sample and the pistons at high temperature. To account for the significant compaction undergone by the pressure assembly, the lower alumina piston is relatively short and a crushable alumina end piece is added at the base of the column. Crushable alumina has a porosity of 40% and is initially very soft. Upon compression, it becomes dense and makes a good piston material.

The procedure consists of increasing the pressure first (within 3 to 4 h) at room temperature. During this cold compression stage, the size of the MgO octahedron decreases considerably (e.g., 20% shortening) because of the collapse of its porosity, and flows between the WC cubes. The extruded material, together with the pyrophyllite, forms the gaskets that contain the pressure medium. The pistons and sample being stiffer than the octahedron materials, high uniaxial stresses develop along the piston-sample column as the octahedron size decreases. After the required pressure is reached, temperature is increased to the desired value

Table 1 Experimental conditions for wadsleyite synthesis in the multianvil apparatus. *Temperatures in italics* correspond to estimations based on calibrations (see text)

Run	Press	Oil pressure (bar)	Pressure (GPa)	Temperature (°C)	Duration (h)	
H1193	Hymag	220	18	*1800–1600*	4	TC broken
S2203	Sumitomo	370	18	*1600–1700*	4	TC broken
H1233	Hymag	220	18	1670	4.5	
S2507	Sumitomo	370	18–19	1500–1550	5	
S2508	Sumitomo	370	18–19	1700–1800	5	

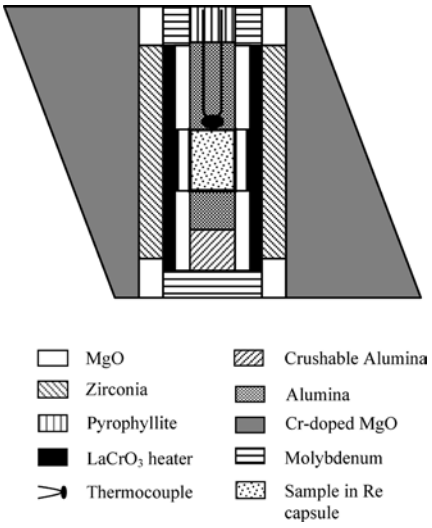

Fig. 1 Schematic of the high-pressure deformation assembly. The specimen is compressed between two hard alumina pistons

at a rate of 50–100 °C min^{-1}. Following an annealing period (usually 30 min to 2 h, although much longer times are possible), the sample is quenched under pressure to <100 °C in 1–2 s by cutting the power to the furnace. Quench rates are fast because of the small size of the pressure cell, which is surrounded by large volumes of metal. Pressure is then decreased slowly to avoid failure of the WC cubes.

Transmission electron microscopy

After completion of the deformation experiment, the sample is recovered and prepared for TEM examination at the University of Lille. The sample capsule is cut into two halves from which two doubly polished thin (25-μm) sections are prepared. The samples are then glued on a Mo grid and ion-milled at 5 kV under a low beam angle of 15° until electron transparency is reached. TEM observations were carried out at 300 kV with a Philips CM30 microscope.

Characterization of dislocation Burgers vectors is difficult with high-pressure phases which are highly beam-sensitive. In the case of wadsleyite, another difficulty arises from the lack of reflections with good structure factors. In the present study, we have analyzed the dislocations by large-angle convergent beam electron diffraction: LACBED (Tanaka et al. 1980; Cherns and Preston 1986; Cherns and Morniroli 1994). This technique is well adapted for defect analysis of irradiation-sensitive materials because only one sample orientation is generally required for determination of the Burgers vector and because the technique uses a defocused electron beam and therefore a low dose of electron irradiation of the specimen. This advantage was clearly demonstrated in the case of quartz (Cordier and Doukhan 1995; Cordier et al. 1995), stishovite (Cordier and Sharp 1998) and majorite garnets (Voegelé et al. 2000).

TEM observations

Sample S2510

The sample shows at the TEM scale clear evidence for plastic deformation. Every grain contains a large density of dislocations (in the range 10^{13} to 10^{14} m^{-2}). Dislocations are sometimes arranged in dense bands as in Fig. 2. In all cases, the dislocation appear to be in glide configuration. Dislocation lines exhibit clear preferred orientations characteristic of a high lattice friction (Fig. 3). Only a few complete Burgers vectors characterizations have been performed on this sample by LACBED, one ⟨101⟩ and five 1/2⟨111⟩ dislocations have been identified. The images reveal that [100](010) and 1/2⟨111⟩{101} slip systems have been activated (three observations in each case).

Sample S2230

All the grains still contain significant dislocation densities (5×10^{13} m^{-2}) but the dense glide bands have disappeared. The dislocations are still in glide configuration. Detailed characterization of dislocation Burgers vectors has been performed by LACBED on 70 dislocations. Four different types of dislocations have been identified: [100] (21 occurrences), 1/2⟨111⟩ (14 occurrences), [010] (9 occurrences, see an example of a LACBED characterization in Fig. 4) and ⟨101⟩ (4 occurrences). In some cases, the glide planes could be identified, leading to the characterization of the following slip systems: [100](001) (4 characterizations), [010](001) (4 characterizations) and 1/2⟨111⟩{101} (4 characterizations). Particular attention has been given to the [010] glide. Elongated [010] dislocation loops with marked edge and screw-preferred orientations are found to glide in (001). The screw segments exhibit a different contrast (Fig. 5). Weak-beam dark-field observations show that these screw segments can be resolved into two or four lines visible with 080. When four lines are visible, they are out of contrast with $g = 303$. The dissociation plane is neither {101} nor (010). When the foil is tilted away from the [001] zone axis (keeping $g = 240$ as a diffraction vector), the edge segment appears to be dissociated either into four partials which exhibit a similar contrast (Fig. 5b), the partials being in contrast with $g = 080$ and out of contrast with $g = 400$. The other types of dislocations

Table 2 Experimental conditions for plastic deformation experiments in the multianvil apparatus. *Italics*: see Table 1

Run	Press	Oil pressure (bar)	Pressure (GPa)	Temperature (°C)	Duration (min)	Sample	
S2510	Sumitomo	380	19	RT	–	S2507	Not heated
S2230	Sumitomo	250	15	1000	90	H1193	
S2228	Sumitomo	300	17	1500–1600	60	S2203	TC uncertain
H1260	Hymag	228	19	*1800–2000*	10	H1233	No TC
H1433	Hymag	220	18	1600	120	S2508	

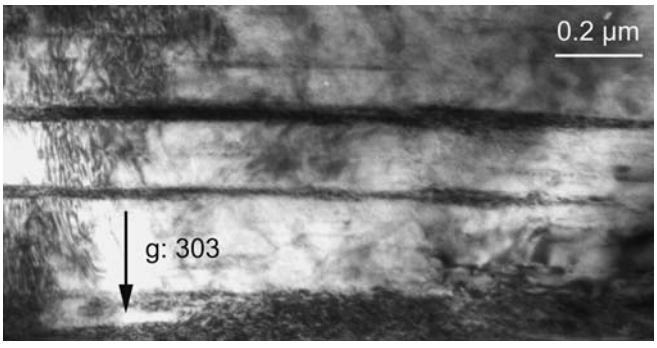

Fig. 2 Sample S2510. Deformation bands parallel to {101} seen edge-on. Bright field *g*: 303

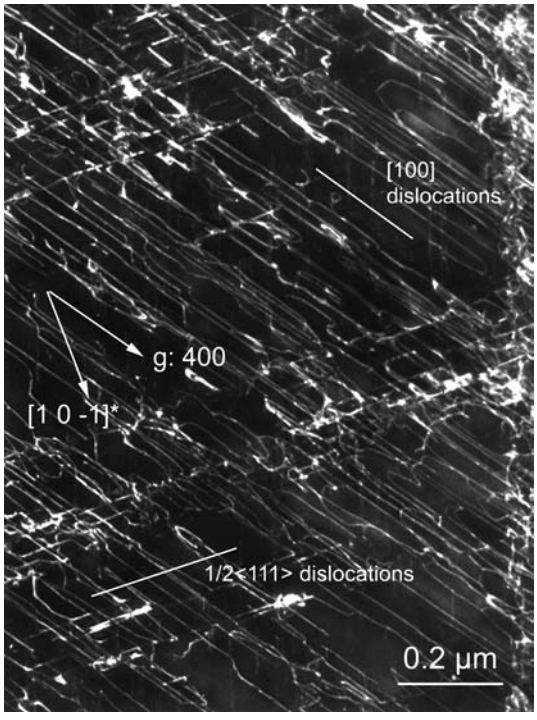

Fig. 3 Sample S2510. Dislocations $1/2\langle 111\rangle$ and [100] in glide configuration. They can be distinguished on the picture from their dominant line directions. Some [010] dislocations can be seen (*vertical lines*) because of their residual contrast. Weak-beam dark field *g*: 400

are difficult to identify in image because of the lack of diffraction vectors and because many slip systems are activated simultaneously. [100] dislocations show no strong preferred orientations. They glide in (001). $1/2\langle 111\rangle$ dislocations have only rarely been identified in image mode. They appear to be dissociated into two partials with similar contrasts and which are visible with $g = 080$, $g = 004$, $g = 400$ and $g = 303$ diffraction vectors. Their glide planes are compatible with {101}.

Sample S2228

In this specimen, very different microstructures can be found from one grain to another. Some grains are

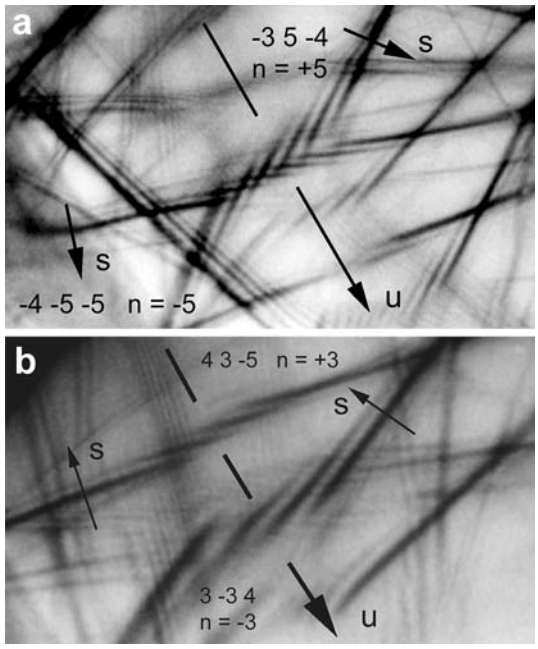

Fig. 4a,b Sample S2230. Characterization by LACBED of a [010] dislocation. The dislocation line is crossed with the *–3 5 –4*, 3 16 3 and *–4 –5 –5* Bragg lines close to the [1154 –22 –914] orientation

pristine, while others contain microstructures very similar to those described earlier with dislocations in glide configuration and dislocation densities of the order of 10^{13} m^{-2}. Seventy dislocations have been characterized by LACBED in 9 different grains. One finds 36 $1/2\langle 111\rangle$ dislocations, 22 [100] dislocations, 5 [001] dislocations, 4 [010] dislocations and 3 $\langle 101\rangle$ dislocations. The slip system $1/2\langle 111\rangle\{101\}$ has been characterized three times. These dislocations are found to be dissociated in their glide plane with a separation between the two identical partials of the order of 15 nm. Evidence for a wide dissociation of [010] dislocations into four partials is shown Fig. 6. The partial separation varies considerably with the dislocation character, being maximum (of the order of 200 nm) for the screw direction. Some grains show stacking faults (Fig. 7) lying in (010). These faults are connected with partial dislocations which are visible with $g = 211$ (Fig. 7b) and out of contrast with $g = 080$ and $g = 303$. They are thus compatible with $1/2\langle 101\rangle$ dislocations. Finally, most deformed grains contain entangled dislocations, junctions and even quite well-organized subgrain boundaries (Fig. 8).

Sample H1433

The microstructures in this sample are heterogenous with some grains left pristine and others highly deformed. Three $1/2\langle 111\rangle$ and three [100] dislocations have been characterized by LACBED in this sample. The dislocations being frequently organized within glide

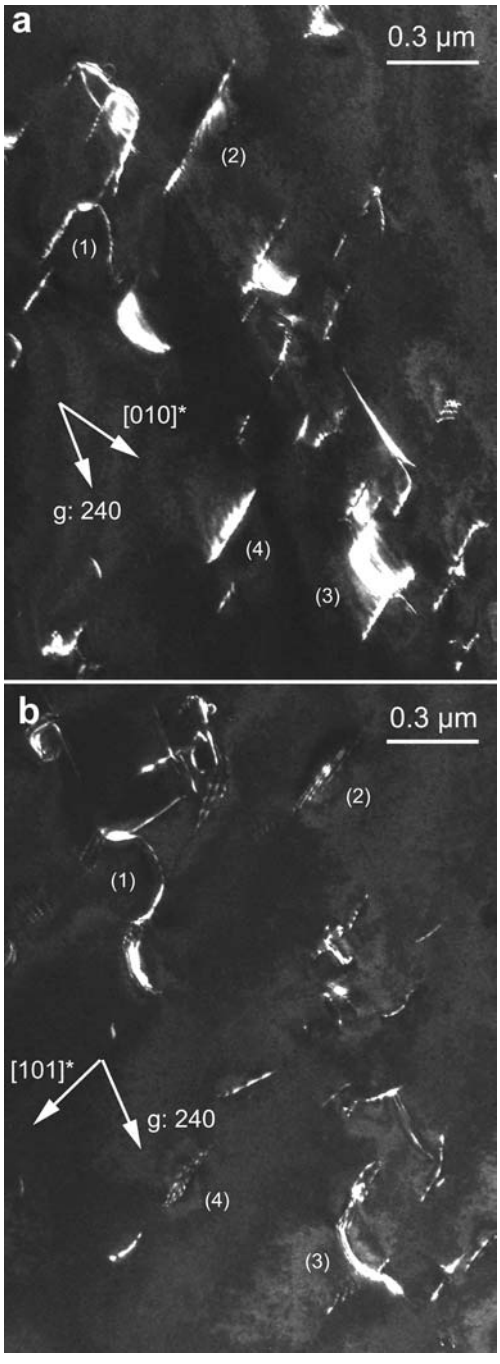

Fig. 5a,b Sample S2230. **a** [010] dislocations viewed along [001]. The screw segments have a more marked contrast than the edge segments. Weak-beam dark field, *g*: 240. **b** Same area after tilting around 240. The edge segments appear to be dissociated into four partials (see dislocations *2* and *4*). Weak-beam dark field, *g*: 240

bands, we have been able to characterize their slip systems. The following slip systems were unambiguously identified: $1/2\langle 111\rangle\{101\}$ (Fig. 9), [100](021) (Fig. 10). Observations compatible with [100](001) and [010]{101} have also been performed. In several grains, the $1/2\langle 111\rangle$ dislocations appeared to be dissociated into two partials (Fig. 11).

Sample H1260

This sample appears to be highly deformed. The grains usually contain a high dislocation density (5×10^{13} m^{-2}), as shown in Fig. 12. Dislocations are in glide configuration, no subgrain boundaries were detected. Fifty one dislocations have been characterized by LACBED: 17 [100] dislocations, 17 [010] dislocations, 16 $1/2\langle 111\rangle$ dislocations and 5 $\langle 101\rangle$ dislocations. In image mode, we have identified the following slip systems: $1/2\langle 111\rangle\{101\}$ (4 occurrences), [100](010) (3 occurrences), [010](001) (1 occurrence), [010]{101} (1 occurrence) and $\langle 101\rangle$ (010) (1 occurrence). As usually the [100] dislocations exhibit straight screw segments (Fig. 13), the [010] dislocations show splitting into four lines (see Fig. 12), and the $1/2\langle 111\rangle$ dislocations are dissociated into two partials.

Discussion

Dislocations and slip systems

Five different types of dislocation Burgers vectors have been identified in this study: $1/2\langle 111\rangle$ (74 characterizations), [100] (63), [010] (30), $\langle 101\rangle$ (13) and [001] (5 characterizations, in one sample only). It is important at this stage to remember that wadsleyite has an orthorhombic structure (space group *Imma*) with the following cell parameters: $a = 5.704$ Å, $b = 11.453$ Å, $c = 8.268$ Å, as determined by Finger et al. 1993 for the $(Mg_{0.92}Fe_{0.08})_2SiO_4$ composition. As a first approximation, the elastic energy per unit length of a dislocation line can be estimated from μb^2, where μ is the shear modulus and b the modulus of the Burgers vector (a more detailed analysis based on anisotropic elasticity will be presented in Part III of this study). This implies that the most favourable dislocations are those corresponding to the shortest lattice repeats. The length of the Burgers vectors of the various dislocations encountered in this study are presented Table 3. The ubiquitous character of [100] and $1/2\langle 111\rangle$ dislocations could be expected from the elastic energy analysis: they correspond to the shortest Burgers vectors. Surprisingly, [001] dislocations have been observed in only one sample while more energetic dislocations such as $\langle 101\rangle$ or [010] dislocations have been found in each sample.

[100] dislocations have already been reported in wadsleyite by Dupas et al. (1994, 1998) and by Sharp et al. (1994). Both authors emphasize the importance of these dislocations for the deformation of wadsleyite. Dupas et al. (1994) identified (021) as a slip system for [100] dislocations, while Sharp et al. (1994) found them gliding in (010). The present study confirms and expands these observations as (001), {011}, (010) and {021} have been identified as possible glide planes for the [100] dislocations. These dislocations usually appear as straight screw segments experiencing high lattice friction.

Fig. 6 Sample S2228. [010] dislocations with screw segments dissociated into four partials. Weak-beam dark field *g*: 240

The edge segments are more mobile and can hardly be seen on the micrographs. This suggests that [100] slip is controlled by the glide of the less mobile, screw segments.

$1/2\langle 111\rangle$ slip has been observed extensively in every sample, suggesting that it plays an important role in the deformation of wadsleyite. The glide planes for these dislocations are {101}; they have been independently characterized 17 times. This observation was expected, as $1/2\langle 111\rangle$ is one of the shortest lattice repeats and {101} are dense planes of the oxygen sub lattice. Indeed, this slip system has already been reported by Dupas et al. (1994). Following these authors, we also found considerable evidence for dissociation of $1/2\langle 111\rangle$ dislocations into two partials. The Burgers vector of the partial dislocations could not be unambiguously identified, but both partials exhibit the same contrast, and are visible

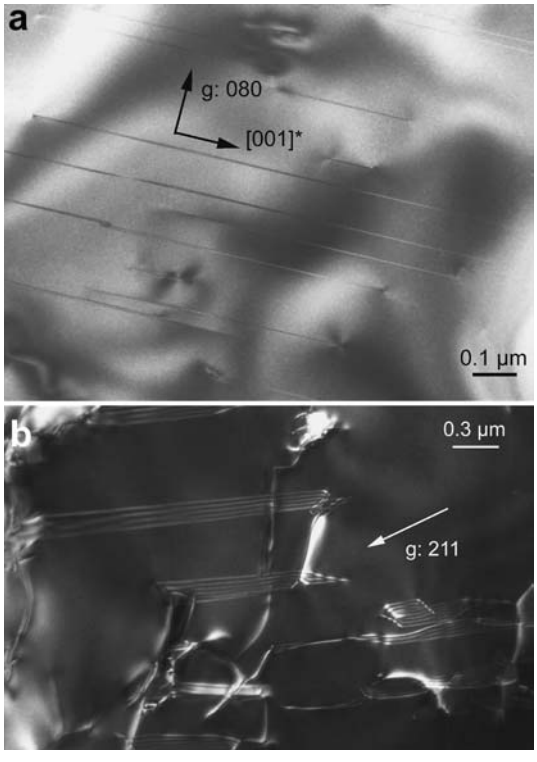

Fig. 7a,b Sample S2228. **a** Stacking faults lying in (010). Bright field *g*: 080. **b** When the specimen is tilted, one can see the fringe contrast of the stacking fault as well as the partial dislocations bounding the faults. Weak-beam dark field *g*: 211

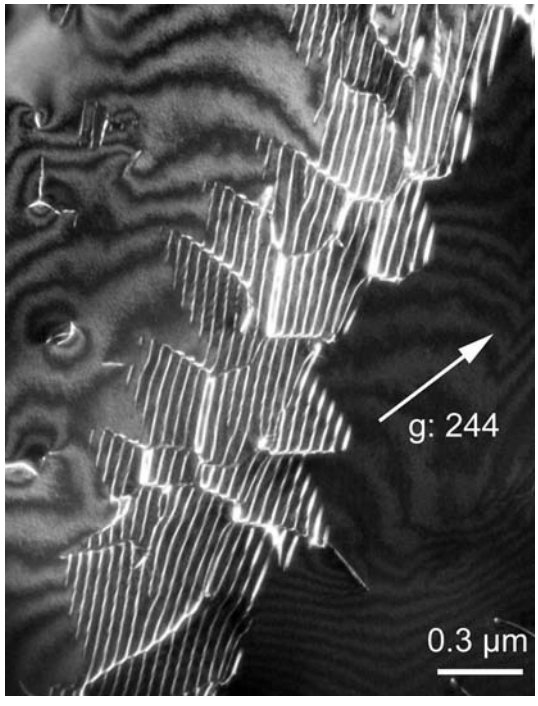

Fig. 8 Sample S2228. Some grains present a very different microstructure dominated by subgrain boundaries. Weak-beam dark-field *g*: 244

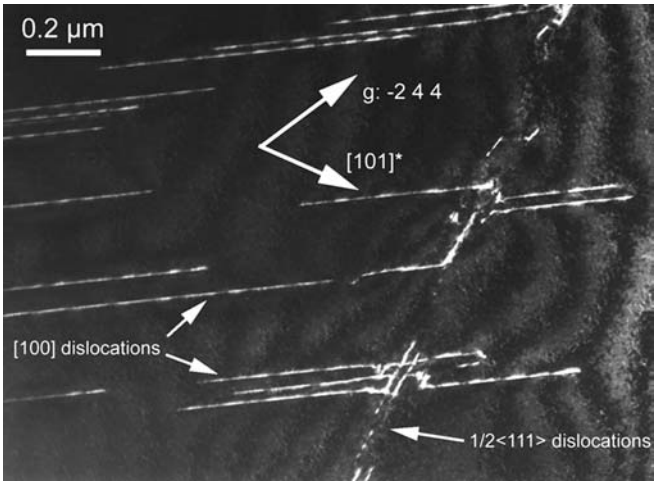

Fig. 9 Sample H1433. Two slip systems intersecting: *[100] dislocations* and *1/2⟨111⟩ dislocations* gliding in a {101} plane (seen edge-on). Weak-beam dark field *g*: 244

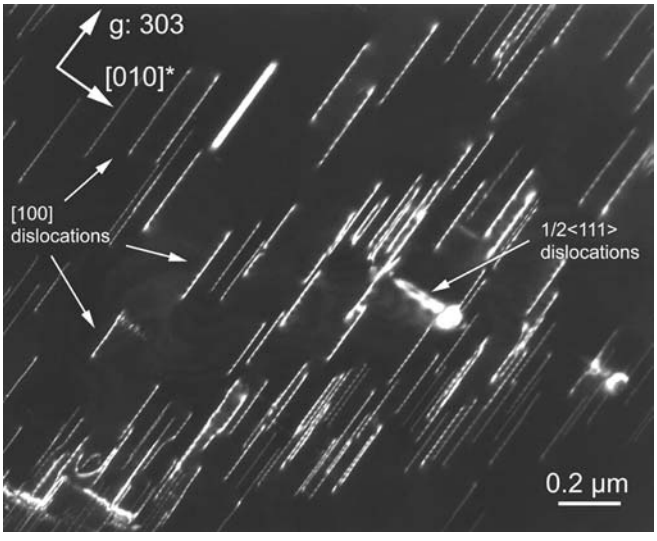

Fig. 10 Sample H1433. *[100] dislocations* gliding in (021). Weak-beam dark field *g*: 303

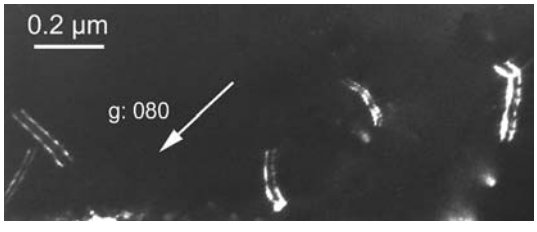

Fig. 11 Sample H1433. 1/2⟨111⟩ dislocations dissociated into two partials. Weak-beam dark field *g*: 080

with 400, 080, 004 and 303 diffraction vectors. This leads us to propose the simple dissociation scheme: $1/2[111] \rightarrow 1/4[111] + 1/4[111]$.

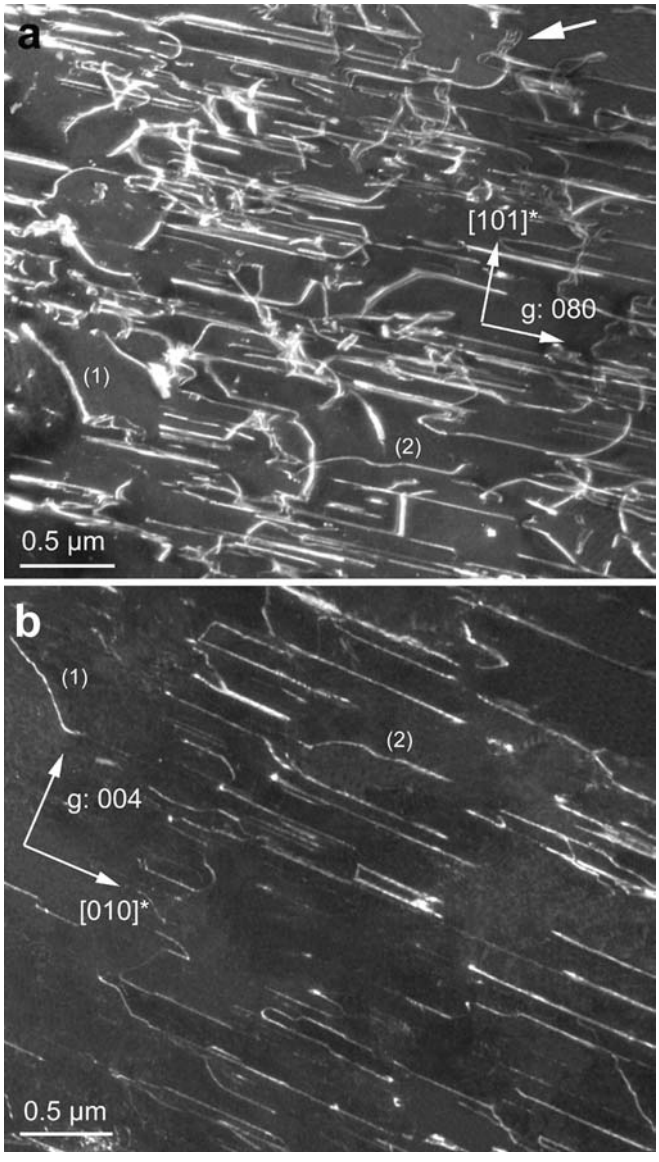

Fig. 12a,b Sample H1260. **a** High density of [010] (note the dissociation in four partials, an example is *arrowed*) and 1/2⟨111⟩ dislocations in glide configuration. Weak-beam dark field *g*: 080. **b** Same area imaged with *g*: 004. The [010] dislocations are no more visible. Weak-beam dark-field

The case of [001] dislocations is more puzzling. Although they have elastic energies only slightly superior to 1/2⟨111⟩ dislocations, and significantly inferior to ⟨101⟩ and [010] dislocations, they have only been rarely observed in this study. In fact, only one sample (S2228) showed evidence for [001] dislocations. It is to be remembered that this sample exhibits very distinctive microstructures with pervasive subgrain boundaries. Indeed, the [001] dislocations have been characterized by LACBED in connection with subgrain boundaries. Unfortunately, they have never been unambiguously identified in image. At this stage, we suppose that the [001] dislocations would be the product of reactions among 1/2⟨111⟩ or ⟨101⟩ dislocations. We note that these

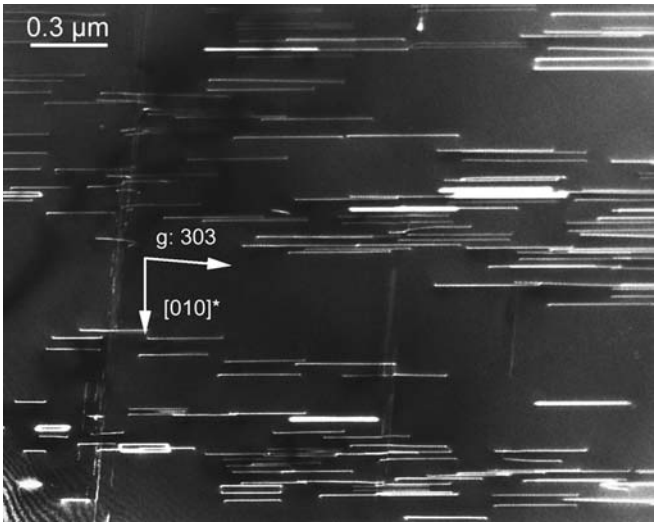

Fig. 13 [100] dislocations gliding in (010). Some [010] dislocations gliding in (101) can be seen through their residual contrast. Weak-beam dark field *g*: 303

Table 3 Burgers vector modulus and elastic energy of the various dislocations characterized in wadsleyite

Burgers vector	Modulus (Å)	μb^2 (Pa m^2)	Relative elastic energy
[100]	5.70	4.06×10^{-8}	1
1/2⟨111⟩	7.62	7.25×10^{-8}	1.8
[001]	8.27	8.55×10^{-8}	2.1
⟨101⟩	10.04	1.26×10^{-7}	3.1
[010]	11.45	1.70×10^{-7}	4.2

dislocations have never been unambiguously characterized in previous studies either. Sharp et al. (1994) suggested that they might be at the origin of 1/2⟨101⟩ dislocations, but they did not identify them.

⟨101⟩ slip has been characterized unambiguously by LACBED (13 occurrences) although those dislocations have been only rarely identified in image. We have observed staking faults in (010) bounded by partial dislocations, the contrast of which is compatible with 1/2⟨101⟩ (Fig. 7b). The fault widths are very variable (up to several μm). It cannot be decided from the observed microstructures whether they result from the splitting of ⟨101⟩ perfect dislocations into two partials, or whether partial 1/2⟨101⟩ dislocations loops have been directly nucleated.

[010] dislocations have been characterized and observed in every sample but one: H1433. These dislocations have been found to glide into two types of planes: (001) and {101}. They are usually easy to distinguish on the images because they form loops with marked screw and edge character. Their contrast is usually very strong, and they exhibit complex splittings into two or four lines. Although we have not undertaken a systematic study of the various dissociation schemes, our observations suggest that: (1) screw segments can decompose into two 1/2⟨111⟩ dislocations gliding in a {101} plane (Fig. 5); (2) screw segments can dissociate into four gliding partials the contrast of which is compatible with 1/4[010] (Fig. 6); (3) edge segments can dissociate into 1/4[010] partials in a climb configuration (Fig. 5). All these reactions result from the instability of [010] dislocations which is predicted by the Frank criterion (based on energetic considerations). A more detailed analysis of these aspects is presented in Part III of this study. It seems thus very unlikely that [010] dislocations glided in their present configuration (in most cases, the dissociation/decomposition takes place in a plane different from the gliding plane of the [010] dislocation). This suggests that [010] slip did occur at an early stage of the experiment. Then, dislocations stopped gliding and relaxed to a more favourable configuration.

About the deformation experiments

Our deformation experiments are characterized by three major parameters: pressure, temperature and time duration. In a multianvil experiment, pressure is usually not controlled directly during the run. It is monitored through the oil pressure applied to the ram (Tables 1, 2). The relationship between the oil pressure and the actual pressure within the assembly relies on calibrations. It is important to note that no specific calibration has been performed for the modified assembly. The pressure values indicated in Tables 1 and 2 have been deduced from calibrations performed with standard 10/5 assemblies. The role of pressure in our experiments is to bring the specimens in the stability field of wadsleyite. This explains the evolution of pressure with temperature which is meant to follow the shape of the stability field of wadsleyite in P, T space. In every experiment, the desired phase has been reached and kept, as checked by TEM on recovered specimens, which validates our experimental conditions.

Temperature is, on the other hand, a parameter than can be followed during the experiment by introduction of a thermocouple close to the specimen. The main source of uncertainty comes from the temperature gradient within the cell. A slight displacement of the thermocouple from its normal position could lead to an over- or underestimation of the actual temperature of the specimen. Another source of uncertainty might come from the failure of the thermocouple (or, as in the case of experiment H1260, from the absence of a thermocouple). In that case, the temperature is deduced from the electrical power (W) delivered to the furnace, which is compared with data collected for numerous previous experiments. The temperature range displayed in Tables 1 and 2 represent the maximum uncertainty deduced from those experiments.

The third parameter is time duration. It has to be chosen a priori. It is to be remembered that our experiments cannot produce strain continuously. The ideal view about this experiment is that the deformation

results from the high elastic stresses built up during compression at room temperature of the anisotropic assembly, as suggested by Durham and Rubie (1997). Then, when the assembly is heated, stresses are relaxed by plastic deformation (Fig. 14). This scenario has been found to operate in the case of garnet deformation (Voegelé et al. 1998). The strain rate decreases with time as in any relaxation test. It is then likely that after a given time, plastic deformation no longer occurs and that temperature only assists recovery (Fig. 14). The time duration can thus have an important effect on the observed microstructures (deformation- or recovery-dominated). It is the reason why, except for sample H1433, the time duration was decreased when temperature was increased.

All our samples show clear microstructural evidence that plastic deformation has been induced. Large densities of dislocations in glide configurations are found in most of the grains. Let us summarize the major characteristics of the microstructure observed. Sample S2230 is highly deformed (high dislocation densities) with several slip systems operating in every grain. One observes numerous [010] dislocations which exhibit evidence for microstructural relaxation (decomposition of screw segments in $1/2\langle 111\rangle$, dissociation outside the glide plane, etc.). S2228 shows also a lot of gliding dislocations, with maybe less [010] dislocations. The principal characteristic of this sample is that it shows evidence of recovery (junctions, subgrain boundaries). H1433 looks very much like S2228, except that it contains no subgrain boundaries nor junctions. Again, one finds in H1460 a dense and complex microstructure with numerous [010] dislocations. It appears clearly that these samples do not constitute a series for which the microstructures would be dominated by temperature. Subgrain boundaries, which are usually regarded as evidence for climb, are present in the sample deformed at about 1500 °C and disappear in samples deformed at higher temperatures. Taking time duration into account can rationalize the differences between samples S2228 and H1260. The microstructure is less relaxed in the former because time duration is much shorter, also temperature is higher. It makes it possible also to understand why samples corresponding to very different temperatures (like S2230 and H1260) exhibit comparable microstructures. However, the differences in microstructures between S2228 and H1433 remain unexplained. Further insights can be provided by the observation of S2510. This sample has been compressed in a way similar to the others, but it has not been heated. According to the simple scenario depicted in Fig. 14, it should have been elastically stressed only. This hypothesis is denied by the TEM investigation, which shows unambiguous evidence for pervasive plastic deformation in this sample. Contrary to garnets (Voegelé et al. 1998), wadsleyite is not strong enough to support the load applied during cold compression. Indeed, it was observed that in garnets, plastic deformation in the low-temperature regime was connected with microcracks introduced during cold compression. We have never observed in wadsleyite any relationship between plasticity and microcracks.

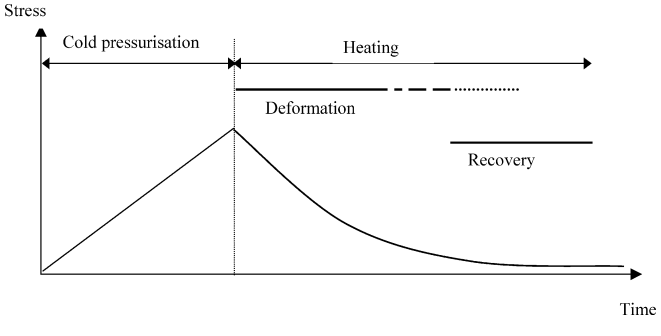

Fig. 14 Model for the stress evolution with time during a compression deformation experiment in the multianvil apparatus. The stresses are built up during cold compression. Plastic deformation takes place only when the specimen is heating. The stresses are then relaxed and recovery tends to dominate when the strain rate becomes too small

These observations lead us to abandon the scenario of Fig. 14, and to tentatively propose the following one. The differential stresses generated during cold compression induce plastic deformation of wadsleyite. The stress level which is reached is thus limited by the strength of the sample (Fig. 15). When temperature is increased, the microstructure introduced at low temperature relaxes and some new plastic deformation (dislocation multiplication and propagation) might occur. However, the starting level of the differential stresses being lower, the deformation might stop relatively early, and then recovery is the only active mechanism. [010] dislocations appeared to be good markers of the thermomechanical history of the samples. These unstable dislocations are likely to have been generated at high stresses and low temperature (during cold compression). They are mostly observed in samples for which restoration was limited, either because time was short (H1260) or because temperature was low (S2230). These dislocations also show the clearest evidence for microstructural relaxation.

Stress is not directly accessible in such high-pressure experiments; however, stress estimates can be inferred from the microstructures on recovered specimens. In most studies, stress estimates were based on dislocation densities measurements (e.g., Wang et al. 1988, Ingrin and Liebermann 1989). This method cannot be applied in the present case for two reasons. First, it has been shown that the dislocation microstructure is partly inherited from cold compression. It is thus difficult to ensure that the dislocation density actually represents the stress state during high-temperature deformation. Moreover, there is no stress-dislocation density calibration available for wadsleyite as for olivine. In a recent study (Cordier et al. 2002), we have suggested taking advantage of the dislocation curvatures to infer local stress states in specimens deformed in a multianvil apparatus. The advantage of the technique is that dislocation bending is likely to adjust much more rapidly to

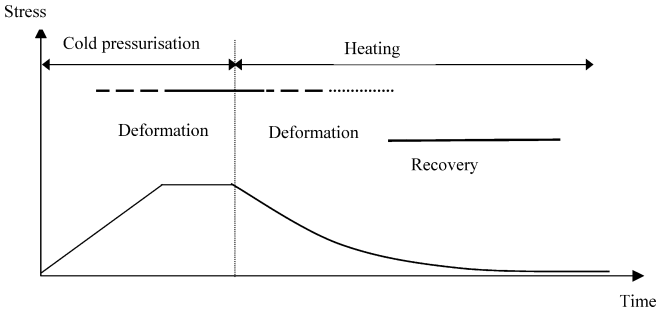

Fig. 15 Model for the stress evolution during the deformation of wadsleyite in the multianvil apparatus. The material is not strong enough to sustain the stress developed during compression and undergoes plastic deformation at room temperature. The stress level is thus limited by the strength of wadsleyite and less deformation is enhanced at high temperature. Recovery is likely to occur more rapidly

stress changes than dislocation density. It must be noted, however, that dislocation curvatures record the last stress state borne by the sample before it is quenched. This technique has been applied to specimens S2230 and S2228, for which the average resolved shear stresses are found to be 400 MPa and 250 MPa, respectively. The difference between both samples is consistent with the different temperatures at which the specimen has been deformed and reflects the decrease of the flow stress with increasing temperature.

Conclusion

Plastic deformation experiments performed on wadsleyite in the multianvil apparatus have allowed characterization of the various dislocations and slip systems that can be activated: $1/2\langle 111\rangle\{101\}$, [100](010), [100](001), [100]{011}, [100]{021}, [010](001), [010]{101} and $\langle 101\rangle$ (010). [001] dislocations have been observed in one specimen only. They are believed to result from dislocation reaction rather than from activation of a slip system. In a number of cases we observed dissociation of dislocations. In particular, [010] dislocations which have a very large Burgers vector are found to decompose in two $1/2\langle 111\rangle$ dislocations or to dissociate into four partial dislocations with 1/4[010] as a possible Burgers vector.

Contrary to garnets, wadsleyite undergoes significant plastic deformation during cold compression in the multianvil apparatus. The microstructures observed post mortem at the TEM are thus the result of this cold compression and of the high-temperature episode. In particular, the [010] dislocations show clear evidence for microstructure relaxation. As a consequence, it is difficult to gain unambiguous information from these experiments on the mechanisms activated at a given temperature.

Acknowledgements High-pressure experiments were performed at the Bayerisches Geoinstitut under the EU IHP – Access to Research Infrastructures Programme (Contract no. HPRI-1999-CT-00004 to D.C. Rubie). P.C. has benefited from a Congé thématique pour recherche from the University of Lille, and would like to thank warmly all the people in Bayreuth who contributed to this work by daily assistance and discussions: Nathalie Bolfan-Casanova, Daniel Frost, Jed L. Mosenfelder and Brent Poe. The quality of the preparation of the TEM specimens by H. Schultze is greatly appreciated.

References

Ando J, Irifune T, Takeshita T, Fujino K (1997) Evaluation of the non-hydrostatic stress produced in a multi-anvil high pressure apparatus. Phys Chem Miner 24(2): 139–148

Bussod GY, Katsura T, Rubie DC (1993) The large-volume multi-anvil press as a high *P–T* deformation apparatus. Pure Appl Geophys 141: 579–599

Chen JH, Inoue T, Weidner DJ, Wu YJ, Vaughan MT (1998) Strength and water weakening of mantle minerals, olivine, wadsleyite and ringwoodite. Geophys Res Lett 25(4): 575–578

Cherns D, Preston AR (1986) Convergent-beam diffraction of crystal defects. Proceedings 11th International Congress on Electron Microscopy, Kyoto, pp 721

Cherns D, Morniroli JP (1994) Analysis of partial and stair-rod dislocations by large angle convergent beam electron diffraction. Ultramicroscopy 53(2): 167–180

Cordier P, Doukhan JC (1995) Plasticity and dissociation of dislocations in water-poor quartz. Phil Mag (A) 72(2): 497–514

Cordier P, Morniroli JP, Cherns D (1995) Characterization of crystal defects in quartz by large-angle convergent-beam electron diffraction. Phil Mag (A) 72(5): 1421–1430

Cordier P, Raterron P, Wang Y (1996) TEM investigation of dislocation microstructure of experimentally deformed silicate garnet. Phys Earth Planet Int 97: 121–131

Cordier P, Sharp TG (1998) Large-angle convergent beam electron diffraction determinations of dislocation Burgers vectors in synthetic stishovite. Phys Chem Miner 25(8): 548–555

Cordier P, Rubie DC (2001) Plastic deformation of minerals under extreme pressure using a multi-anvil apparatus. Mat Sci Eng (A) 309–310: 38–83

Cordier P, Thurel E, Rabier J (2002) Stress determination in multianvil deformation experiments based on dislocation curvatures measurements: Application to wadsleyite and ringwoodite – art. no. 1354. Geophysical Research Letters 29(9): 1354

Dupas C, Doukhan N, Doukhan JC, Green II HW, Young TE (1994) Analytical electron microscopy of a synthetic peridotite experimentally deformed in the b olivine stability field. J Geophys Res 99(B8): 15821–15832

Dupas-Bruzek C, Sharp TG, Rubie DC, Durham WB (1998) Mechanisms of transformation and deformation in $Mg_{1.8}Fe_{0.2}SiO_4$ olivine and wadsleyite under non-hydrostatic stress. Phys Earth Planet Interiors 108(1): 33–48

Durham WB, Rubie DC (1997) Can the multianvil apparatus really be used for high-pressure deformation experiments? In: Properties of Earth and Planetary Materials at High Pressure and Temperature 101: 63–70

Finger LW, Hazen MH, Zhang J, Ko J, Navrotski A (1993) The effect of Fe on the crystal structure of wadsleyite β-$(Mg_{1-x}Fe_x)_2SiO_4$ $0.00 \le x \le 0.40$. Phys Chem Miner 19: 361–368

Fujimura A, Endo S, Kato M, Kumazawa M (1981) Preferred orientation of beta-Mn_2GeO_4. Seismol Soc Jpn, pp 185

Green II HW, Young TE, Walker D, Scholz CH (1990) Anticrack-associated faulting at very high pressure in natural olivine. Nature 348(6303): 720–722

Ingrin J, Liebermann RC (1989) Deviatoric stress in a girdle-anvil type high-pressure apparatus: effect on the quartz-coesite phase transformation. Physics of the Earth and Planetary Interiors 54: 378–385

Karato S, Dupas-Bruzek C, Rubie DC (1998) Plastic deformation of silicate spinel under the transition-zone conditions of the Earth's mantle. Nature 395(6699): 266–269

Karato S, Rubie DC (1997) Toward an experimental study of deep mantle rheology: a new multianvil sample assembly for deformation studies under high pressures and temperatures. J Geophys Res Solid Earth 102(B9): 20111–20122

Kawai N, Endo S (1970) The generation of ultrahigh hydrostatic pressure by a split sphere apparatus. Rev Sci Instrum 41: 1178–1181

Liebermann RC, Wang Y (1992) Characterization of sample environment in a uniaxial split-sphere apparatus. In: Syono Y, Manghnani MH (eds) High-pressure research: application to Earth and planetary sciences. American Geophysical Union, Washington, DC, pp 19–31

Mosenfelder JL, Connolly JAD, Rubie DC, Liu M (2000) Strength of $(Mg,Fe)_2SiO_4$ wadsleyite determined by relaxation of transformation stress. Phys Earth Planet Inter 120(1–2): 63–78

Rubie DC (1999) Characterizing the sample environment in multianvil high-pressure experiments. Phase Transitions 68: 431–451

Sharp TG, Bussod GY, Katsura T (1994) Microstructures in β-$Mg_{1.8}Fe_{0.2}SiO_4$ experimentally deformed at transition-zone conditions. Phys Earth Planet Int 86: 69–83

Tanaka M, Saito R, Ueno K, Harada Y (1980) LACBED. J Elec Microsc 29(4): 408–412

Voegelé V, Ando JI, Cordier P, Liebermann RC (1998) Plastic deformation of silicate garnets I. High-pressure experiments. Phys Earth Planet Inter 108(4): 305–318

Voegelé V, Cordier P, Langenhorst F, Heinemann S (2000) Dislocations in meteoritic and synthetic majorite garnets. Eur J Mineral 12(4): 695–702

Wang Y, Liebermann RC, Boland JN (1988) Olivine as an in situ piezometer in high pressure apparatus. Physics and Chemistry of Minerals 15: 493–497

Weidner DJ, Wang Y, Vaughan MT (1994) Yield strength at high pressure and temperature. Geophys Res Lett 21(9): 753–756